

PACS numbers: 07.57.Hm; 42.30.Wb; 42.25.Kb
DOI: 10.1070/QE2015v045n10ABEH015468

Low-coherence terahertz tomography based on spatially separated counterpropagating beams with allowance for probe radiation absorption in the medium

V.I. Mandrosov

Abstract. **This paper analyses low-coherence tomography of absorbing media with the use of spatially separated counterpropagating object and reference beams. A probe radiation source based on a broadband terahertz (THz) generator that emits sufficiently intense THz waves in the spectral range 90–350 μm and a prism spectroscope that separates out eight narrow intervals from this range are proposed for implementing this method. This allows media of interest to be examined by low-coherence tomography with counterpropagating beams in each interval. It is shown that, according to the Rayleigh criterion, the method is capable of resolving inhomogeneities with a size near one quarter of the coherence length of the probe radiation. In addition, the proposed tomograph configuration allows one to determine the average surface asperity slope and the refractive index and absorption coefficient of inhomogeneities 180 to 700 μm in size, and obtain spectra of such inhomogeneities in order to determine their chemical composition.**

Keywords: *terahertz radiation, coherence, tomography.*

1. Introduction

A great deal of attention is currently paid to promising optical low-coherence tomography techniques [1–4], in which a medium to be investigated is probed by low-coherence light and the wave scattered by the medium interferes with a reference wave, which copropagates with the object wave. The full width at half maximum (FWHM) of the coherence function, which determines the resolving power of such techniques, is then equal to the coherence length of the probe light [3], i.e. using techniques described in Refs [1–4] one can identify inhomogeneities whose length scale is comparable to the coherence length of the probe light. In a recent study [5], an optical low-coherence tomography technique has been proposed which utilises focused-image holography [6] with an object beam and reference beam counterpropagating at an obtuse angle to each other. This ensures almost a factor of 2 better resolving power, so the technique makes it possible to resolve finer inhomogeneities in media.

The main drawback of the techniques proposed in Refs [1–5] is that they have not been adapted to spectroscopy of media and have been used to analyse the structure of media in a single, rather narrow spectral band. Moreover, the visible or IR probe light used in these techniques rules out investigation of media opaque in these spectral ranges.

Cherkasova et al. [7] proposed low-coherence tomography with terahertz (THz) probe radiation (in the range 60–600 μm) using an object and a reference beam also making an obtuse angle with each other. This approach also ensures almost a factor of 2 better resolving power. The use of radiation in the spectral range 60–600 μm opens up wide possibilities for the study of inhomogeneities in biological media, such as sugars, fats, haemoglobin and dental tissue, as well as for the spectroscopic determination of their chemical composition [8], which is usually impossible in the case of visible and near-IR probe light. As a low-coherence radiation source, Cherkasova et al. [7] proposed a device which included a broadband THz generator and a reflective diffraction grating that formed THz probe radiation with a coherence length 8λ (where λ is the average wavelength of the radiation) in a sufficiently narrow range of diffraction angles. As shown by Bakut and Mandrosov [9], this is the minimum coherence length of probe radiation that can be used for gaining information about objects by virtue of the coherence properties of the radiation. As a result, the resolving power approaches its limit.

Kuritsyn et al. [10] proposed a low-coherence THz tomograph scheme based on spatially separated counterpropagating beams, using probe radiation with a coherence length 8λ and Denisyuk's focused-image holography scheme [11]. As shown by them [10], this ensures the highest possible resolving power, which allows one to resolve inhomogeneities about 2λ in size. This means in particular that, if this method were implemented in the optical spectral region, its resolving power would be a factor of 2 better than that of the techniques considered in Refs [1–4]. In the method proposed by Kuritsyn et al. [10] a tomogram of a medium can be obtained by recording instantaneous field amplitudes in the two counterpropagating beams. In the case of layered media, such a tomogram can be used e.g. to determine the refractive index in each layer, the average slope of asperities on the surface of the layers and their thickness and depth with the highest possible resolving power, which may, according to the Rayleigh criterion, reach one quarter of the coherence length of the probe radiation. If the coherence length of probe radiation is 8λ, the resolving power is 2λ.

The main drawback of the methods considered in Refs [7, 10] is that the probe radiation source proposed in those studies is unsuitable for effective separation of several narrow low-coherence emission bands with different centre wavelengths from broadband THz radiation. This makes it impossible to obtain, in addition to tomograms of media, information about their spectra. For example, when low-

V.I. Mandrosov Moscow Institute of Physics and Technology (State University), Institutskii per. 9, 141700 Dolgoprudnyi, Moscow region, Russia; e-mail: vmandrosov@mail.ru

Received 17 March 2015; revision received 12 July 2015
Kvantovaya Elektronika **45** (10) 959–964 (2015)
Translated by O.M. Tsarev

coherence probe radiation with a centre wavelength λ is separated out by a reflective diffraction grating from the output of a broadband THz source, rather intense radiation with centre wavelengths from $\lambda/2$ to $3\lambda/2$ may fall in the same diffraction angle. It can be shown that, in such a case, even at a very low noise level it is essentially impossible to extract reliable information about the structure of the medium from its tomogram. It is also worth noting that Kuritsyn et al. [10] analysed only tomograms of media transparent in the THz range.

In this report, probe radiation absorption in the medium is taken into account in analysing tomograms. This allows one, in principle, to obtain almost complete information about the structure of inhomogeneities in media and their chemical composition with the highest possible resolution. A compact low-coherence THz tomograph scheme is presented which takes advantage of spatially separated counterpropagating object and reference beams and ensures the optimal use of the probe radiation energy. To implement this scheme, it is planned to use a low-coherence THz probe radiation source based on a broadband THz generator excited by femtosecond laser pulses, which will make it possible to obtain not only tomograms of media but also their spectra at several wavelengths. In the method presented here, a tomogram will be obtained by recording instantaneous field amplitudes in the two counterpropagating beams. It should be noted that this study is purely theoretical: experimental implementation of a low-coherence THz probe radiation source, which is described in detail in Appendix, is still in the very early stage of development.

2. Compact long-focus, low-coherence THz tomograph scheme based on spatially separated counterpropagating reference and object beams

Figure 1 shows a schematic of the proposed tomograph. A THz source (*1*) in the spectral range 90–350 μm sequentially separates eight narrow regions from this range, with centre wavelengths λ_k, bandwidths $\Delta\lambda_k = \lambda_k/8$ (λ_1 = 100 μm, λ_2 = 113 μm, λ_3 = 128 μm, λ_4 = 148 μm, λ_5 = 174 μm, λ_6 = 209 μm, λ_7 = 262 μm, λ_8 = 329 μm) and electric field components $E_{sk}(t) = E_k U_k(t)$, where E_k is the amplitude of the kth component; $U_k(t) = u_k(t)\cos[\omega_k t + \psi_k(t)]$ is a dimensionless function describing the time variation of this component; $\omega_k = 4\pi c/\lambda_k$ is the high carrier frequency of the radiation; $\psi_k(t)$ is the phase of the kth component (rapidly varying in time); and $u_k(t) \leqslant 1$ is a slowly varying modulation function of this component. As a result, low-coherence probe radiation can be produced at the outer aperture of the source in the form of spherical waves with coherence lengths $L_{ck} = 8\lambda_k$, equal to the minimum coherence lengths that can be used for gaining information about objects by virtue of the coherence properties of the radiation [8] (see Appendix and Fig. 1A for more details).

Without loss of generality, consider the formation of a tomogram with the use of probe radiation at the minimum centre wavelength λ_1 = 100 μm with a coherence length $L_{c1} = 8\lambda_1$ = 800 μm. The radiation from the source (*1*) (Fig. 1) propagates to lens *2*, located a distance $2f_p$ from the source (where f_p is the focal length of the lens), and a parabolic mirror (*3*) with a focal length $f_r = 2f_p$. It is then focused by lens *2* to point A, located two focal lengths ($2f_p$) from the lens. The focused beam probes the boundary layer (*4*) of the medium to be studied (*5*) and its boundary segment (*6*), consisting of several zones (in Fig. 1, segment *6* consists of seven zones).

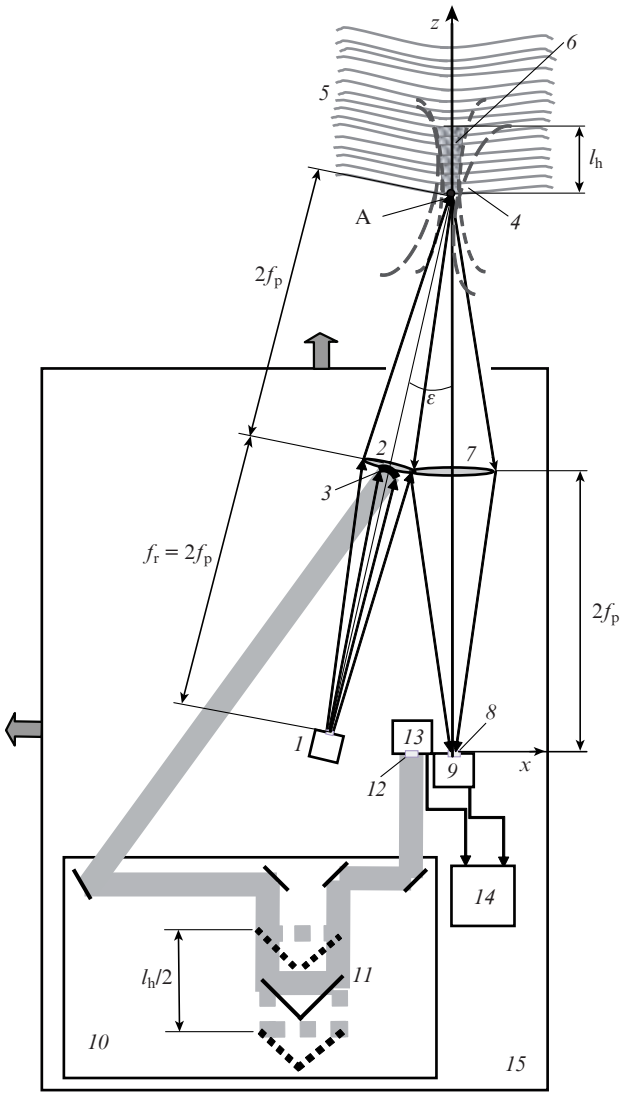

Figure 1. Schematic of the low-coherence THz tomograph based on spatially separated counterpropagating reference and object beams: (*1*) low-coherence source; (*2*, *7*) long-focus lenses; (*3*) parabolic mirror; (*4*) boundary layer of a layered medium (*5*); (*6*) boundary segment of the medium (*5*); (*8*) input aperture of a detector (*9*) of the instantaneous electric field component in an image of different zones of the boundary segment (*6*); (*10*) reference-beam time-delay unit composed of four mirrors and an angular reflector (*11*); (*12*) input aperture of a detector (*13*) of the instantaneous electric field component in the reference beam; (*14*) computer producing a tomogram of the medium (*5*); (*15*) tomograph frame. The long-dashed lines delineate the waist region where the probe radiation energy is concentrated, and the short-dashed lines delineate the region that makes a major contribution to the backscattered radiation energy. The grey arrows indicate the longitudinal and transverse displacement directions of the tomograph frame (*15*). The tomograph frame is in its initial position at the instant when detector *9* records the electric field component in the image of the boundary (*4*) of the medium (*5*).

Near lens *2*, there is lens *7*, placed so that the angle ε between the optical axes of the lenses is 0.1 rad and the focal spot of the probe radiation (A) is a distance $2f_p$ from lens *7*. The diameter of lens *7* is twice that of lens *2*, and its focal length is also f_p. Lens *7* collects the backscattered radiation to form an object beam, which produces a focused image of segment *6* on the input aperture (*8*) of a detector (*9*). The detector records the instantaneous electric field component $E_o(t, x, y, z = 0)$ in

the object beam, where xyz is a coordinate system with its x and y axes lying in the plane of aperture *8* and its z axis directed along the optical axis of lens *7*. The origin ($x = 0$, $y = 0$, $z = 0$) is at the centre of aperture *8*. To simplify subsequent calculations, segment *6* is taken to have the shape of a parallelepiped with a height equal to the longitudinal size of the focal region of the object beam, $l_h = 4\lambda_1(f_p/d)^2$ (where d is the diameter of lens *7*), and a square base with a side length $l_s = 2\lambda_1(f_p/d)$, equal to the transverse size of this region.

Concurrently with the formation of the object beam, a reference beam is formed by the parabolic mirror (*3*) from some of the radiation incident on lens *2*. It has the form of a plane wave, which is directed by the mirror to a delay unit (10) that produces a time delay between the reference and object beams. The unit comprises four mirrors and a mobile angular reflector (*11*). When the reflector is displaced a distance Z from its central position at $Z = 0$ [which corresponds to a propagation time of the reference beam from the source (*1*) to aperture *12* $\tau_r = 4f_p/c$], the time delay is $\tau_{dr}(Z) = 2Z/c$. From the delay unit (*10*), the reference beam propagates in a direction opposite to that of the object beam to the input aperture (*12*) of the detector (*13*) of the instantaneous field amplitude in the reference beam. That the beams propagate in opposite directions ensures the highest possible resolving power of the proposed method: $2\lambda_1$. In the xyz coordinate system, the instantaneous amplitude is

$$E_r(t, x = -\Delta, y, z = 0, Z) = C_r E_l U_l(t + \tau_r - \tau_{dr}),$$

where C_r is a constant; $x = -\Delta$, $y = 0$ and $z = 0$ are the coordinates of the centre of aperture *12*; and Δ is the distance between the centres of the input apertures (*8*, *12*) of the detectors (*9*, *13*). At the extreme positions of the angular reflector (*11*) ($Z = \pm l_h/4$), marked by dashed lines, we have $\tau_{dr}(Z = \pm l_h/4) = \pm l_h/(4c)$. The instantaneous field amplitudes in the reference and object beams, $E_r(t, x = -\Delta, y, z = 0, Z)$ and $E_o(t, x, y, z = 0)$, are fed to a computer (*14*) and are used to compute the intensity distribution in the hologram of the focused image of segment *6*,

$$I_h(t, x, y, z = 0, Z) = [E_r(t, x = -\Delta, y, z = 0, Z = 0) + E_o(t, x, y, z = 0)]^2, \quad (1)$$

and the intensity averaged over the tomogram formation time T,

$$\bar{I}_{hn}(x, y, z = 0, Z) = \left[\frac{1}{T}\int_{t_0}^{t_0+T} I_h(t, x, y, z = 0, Z)\,dt\right] \Big/ (C_r E_l)^2.$$

Here the intensity is normalised to the reference beam power:

$$Q_r = \frac{1}{T}\int_{t_0}^{t_0+T} E_r^2(t, x = -\Delta, y, z = 0, Z)\,dt = (C_r E_l)^2,$$

where t_0 is the instant when the instantaneous amplitude $E_o(t, x, y, z = 0)$ began to be detected. When the reference beam power Q_r considerably exceeds the object beam power,

$$Q_o = \frac{1}{T}\int_{t_0}^{t_0+T} E_o^2(t, x, y, z = 0)\,dt,$$

we have

$$\bar{I}_{hn}(x, y, z = 0, Z) \approx 1 + \frac{2}{T} \times \left[\int_{t_0}^{t_0+T} E_o(t, x, y, z = 0) E_r(t, x = -\Delta, y, z = 0, Z = 0)\,dt\right] \times (C_r E_l)^{-2}. \quad (2)$$

Next, the square of the function $\bar{I}_{hn}(x, y, z = 0, Z)$ is averaged over the area S_a of the input aperture (*12*) of detector *13* in the computer (*14*):

$$\tilde{I}_{hn}(Z) = (1/S_a)\iint \bar{I}_{hn}^2(x, y, z = 0, Z)\,dx\,dy.$$

Using relations (1) and (2) and previous results [10, 12], it can be shown that, if the average asperity slopes γ_b and γ_j between neighbouring layers of a medium under study satisfy the inequalities $\gamma_b \gg d/(2f_p)$ and $\gamma_j \gg d/(2f_p)$, which are usually met in practice, we have

$$\bar{I}_{hn}(Z) \approx 1 + \tilde{k}_b B_{u1}^2(2Z/L_{c1})\cos^2(4\pi Z/\lambda_1) + \sum_{j=1}^{N} \tilde{k}_j B_{u1}^2[2(Z - l_{wj})/L_{c1}]\cos^2[4\pi(Z - l_{wj})/\lambda_1], \quad (3)$$

where

$$\tilde{k}_b = (1/\gamma_b)^2/(n_1 + 1)^2 \ll 1;$$

$$\tilde{k}_j = (1/\gamma_j)^2 \exp(-4\sum_{i=1}^{j} \alpha_i l_i)/(n_j + n_{j+1})^2 \ll 1;$$

$$B_{u1}(\tau) = \frac{1}{T}\int_{t_0}^{t_0+T} u_1(t) u_1(t + \tau)\cos[\psi_1(t) - \psi_1(t + \tau)]\,dt$$

is the coherence function of probe radiation at the centre wavelength $\lambda_1 = 100$ μm; α_i is the absorption coefficient of the ith zone; l_i is the thickness of the ith zone; n_j is the refractive index in the jth zone; and $l_{wj} = \sum_{i=1}^{i=j} l_i n_i$ is the optical path length of the probe beam from the boundary surface of segment *6* to the surface of the jth zone. Assuming that the phase $\psi_1(t)$ is a random process that follows a Gaussian law with a correlation time τ_ψ and standard deviation $\sigma_\psi \gg \pi$, and that $|u_1(t)| = \exp(-t^2/\tau_1^2)$, we obtain $B_{u1}(\tau) = \exp[-(\tau/\tau_{c1})^2]$, where $\tau_{c1} = \sqrt{\tau_1^2 + (\tau_\psi/\sigma_\psi)^2}$, and τ_1 is the FWHM of the modulation function. The parameters $\tilde{k}_b$ and $\tilde{k}_j$ in (3) can be interpreted as the reflectivity of the front surface of the first boundary zone of segment *6* of the medium under investigation and that of the interfaces between the zones of the segment, respectively.

It follows from (3) that the envelope of the function $\tilde{I}_{hn}(Z)$ has the form

$$\tilde{V}_t(Z) = 1 + \tilde{k}_b B_{u1}^2(2Z/L_{c1}) + \sum_{j=1}^{N} \tilde{k}_j B_{u1}^2[2(Z - l_{wj}/2)/L_{c1}], \quad (4)$$

which represents a tomogram of the boundary segment (*6*) of the layered medium (*5*), containing information about the parameters γ_j, α_j, n_j and l_j ($j = 1-N$), which determine the structure of segment *6*. It follows from (4) that the tomogram of segment *6* has maxima at $Z = 0$ and at the boundaries of the

layers ($Z_j = l_{wj}/2$): $\tilde{V}_t(Z = 0) = 1 + \tilde{k}_b$ and $\tilde{V}_t(Z_j) = 1 + \tilde{k}_j$. To find the parameters γ_j, α_j, n_j and l_j of the zones in the boundary segment (*6*), the angular reflector (*11*) is displaced relative to its centre position $Z = 0$ (Fig. 1). In particular, if the reflector (*11*) is displaced from its centre position $Z = 0$ by $Z = Z_2 = l_{w2}/2 = (l_1 n_1 + l_2 n_2)/2$, we have $\tau_{dr}(Z = Z_2) = \tau_r + 2Z_2/c$. The tomogram $\tilde{V}_t(Z)$ then reaches one of its maximum values, $\tilde{V}_t(Z_2) = 1 + \tilde{k}_2$, near which $\tilde{V}_t(Z) \approx 1 + \tilde{k}_2 B_{u1}^2 \times [2(Z - l_{w2}/2)/L_{cl}]$. This relation is the consequence of the fact that, when the source (*1*) has a coherence length $L_{cl} = 8\lambda_1$, the function $B_{u1}^2[2(Z - l_{w2}/2)/L_{cl}]$ becomes so narrow that the other maxima in the tomogram $\tilde{V}_t(Z)$ have a negligible effect on its shape. Physically, this means that, at a low coherence of the source (*1*), $L_{cl} = 8\lambda_1$ and $Z = Z_2$, the rays filtered out from the entire radiation backscattered by segment *6* are those backscattered by the interface between the second and third zones and an adjacent region of the medium (*5*). It can be shown in a similar way that, when the angular reflector (*11*) is displaced from its centre position $Z = 0$ by $Z = Z_j = l_{wj}/2$ and the coherence length of the source is $L_{cl} = 8\lambda_1$, the rays filtered out are those backscattered by the interface between zones j and $j + 1$. We then have $\tilde{V}_t(Z) \approx 1 + \tilde{k}_2 B_{u1}^2 \times [2(Z - l_{wj})/L_{cl}]$.

The above relations can be used to determine parameters of all the zones in segment *6*. For example, to find the properties of zones 1 and 2 and the refractive index of zone 3 (n_3), we use the fact that, when the angular reflector (*11*) is in its central position ($Z = 0$) or is displaced from this position by $Z_1 = l_1 n_1/2$ and $Z_2 = Z_1 + l_2 n_2/2$, the following relations hold:

$$\tilde{V}_t(Z = 0) = 1 + \tilde{k}_b,\ \tilde{V}_t(Z_1) = 1 + \tilde{k}_1, \tilde{V}_t(Z_2) = 1 + \tilde{k}_2, \qquad (5)$$

where $\tilde{k}_b = (1/\gamma_b)^2/(n_1 + 1)^2$; $\tilde{k}_1 = (1/\gamma_1)^2 \exp(-4\alpha_1 l_1)/(n_1 + n_2)^2$; and $\tilde{k}_2 = (1/\gamma_2)^2 \exp[-4(\alpha_1 l_1 + \alpha_2 l_2)]/(n_2 + n_3)^2$.

Since zones 1 and 2 of segment *6* are located in a relatively limited volume (*4*) of the medium (*5*), the average asperity slopes γ_1 and γ_2 on the interfaces between the zones and the absorption coefficients α_1 and α_2 of these zones are very likely to be identical: $\alpha_1 = \alpha_2$ and $\gamma_b = \gamma_1 = \gamma_2$. Given this and using relations (5), we obtain a system of seven equations in seven unknowns (γ_1, l_1, n_1, l_2, n_2, α_1 and n_3):

$$Z_1 = l_1 n_1/2, \quad \tilde{V}_t(Z = 0) = 1 + \tilde{k}_b,$$

$$\tilde{V}_t(Z_1) = 1 + \tilde{k}_1, \quad Z_2 = (l_1 n_1 + l_2 n_2)/2, \qquad (6)$$

$$\tilde{V}_t(Z_0') \approx 1 + \tilde{k}_b/e\,,\ \tilde{V}_t(Z_1') \approx 1 + \tilde{k}_1/e\,,\ \tilde{V}_t(Z_2') \approx 1 + \tilde{k}_2/e\,,$$

where $\tilde{V}_t(Z_0')$, $\tilde{V}_t(Z_1')$ and $\tilde{V}_t(Z_2')$ are the values of the $\tilde{V}_t(Z)$ tomogram at the points $Z_0' = L_{cl}/4$, $Z_1' = Z_1 + L_{cl}/4$ and $Z_2' = Z_2 + L_{cl}/4$; $\tilde{k}_b = (\alpha_1/\gamma_1)^2/(n_1 + 1)^2$; $\tilde{k}_1 = (\alpha_1/\gamma_1)^2 \times \exp(-4\alpha_1 l_1)/(n_1 + n_2)^2$; and $\tilde{k}_2 = (\alpha_1/\gamma_1)^2 \exp[(-4\alpha_1(l_1 + l_2)]/(n_2 + n_3)^2$.

The system of equations (6) is used to compute the parameters γ_1, l_1, n_1, l_2, n_2, n_3 and α_1 in unit *14*. Similarly, displacing the angular reflector (*11*) by $Z_3 + l_3 n_3/2$, $Z_4 = Z_3 + l_4 n_4/2$, $Z_5 = Z_4 + l_5 n_5/2$ and $Z_6 = Z_5 + l_6 n_6/2$ we can find the thicknesses, refractive indices and absorption coefficients of the other four zones in the boundary segment (*6*) and the average asperity slopes on the interfaces between these zones.

The tomograph frame (*15*) is moved in transverse directions over distances that are multiples of the diameter of the minimum cross section of the waist region of lens *7*: $l_s = 2\lambda_1(f_p/d)$. This yields tomograms of all the segments of longitudinal size $l_b = 2\lambda_1(f_p/d)^2$ located at the same depth as the boundary segment. The tomograph frame (*15*) is then displaced over a distance l_b in the longitudinal direction, and a tomogram of a segment neighbouring in depth in the medium (*5*) is produced by the computer (*14*). Next, the tomograph frame (*15*) is again displaced in transverse directions over distances that are multiples of l_s. This yields tomograms of the segments located at the same level as the indicated segment. A similar procedure yields tomograms of segments located at different levels. This means that the proposed type of low-coherence THz tomograph allows one to obtain sufficiently complete information about parameters of arbitrary segments of a medium (*5*).

Evaluated using the Rayleigh criterion, like in a previous study [10], the resolving power of the tomograph under consideration lies in the range 180–700 μm. Therefore, experimental uncertainty in the size of inhomogeneities in the segments, as well as in the distance between the inhomogeneities and the surface of the medium, lies in the same range. Uncertainty in the refractive indices n_j of different layers of the medium (*5*) as determined using the proposed tomograph in the presence of, e.g., additive noise is exactly the same as that reported by Kuritsyn et al. [10].

Uncertainty in the absorption coefficients of inhomogeneities and the average asperity slopes on the boundary (*4*) of the medium (*5*) and on the boundary surfaces of each layer increases with increasing signal-to-noise ratio and decreasing asperity slope on these boundaries. The reason for this is that the lower the asperity slope, the narrower is the cone in which the probe radiation backscattered by the asperities propagates and the larger is the amplitude of the electric field component in the object beam, recorded by detector *9* (Fig. 1).

3. Conclusions

A compact long-focus, low-coherence THz tomograph scheme has been proposed which takes advantage of spatially separated counterpropagating reference and object beams. The tomograph can be used to obtain almost complete information about the structure of inhomogeneous media. In particular, in the case of layered media such a tomograph will make it possible to determine the thickness of each layer, the average asperity slope on the boundaries of individual layers and the refractive indices and absorption coefficients of each layer in the THz range. In the case of a homogeneous medium containing inhomogeneities, a tomograph based on the proposed scheme can be used to determine the refractive index and absorption coefficient of each inhomogeneity in the THz range and the average asperity slope on the surface of the inhomogeneities. Experimental uncertainty in these parameters decreases with increasing signal-to-noise ratio and decreasing average asperity slope on the surface of inhomogeneities in the medium. The inhomogeneity size and the distance between them and the surface of the medium can be determined with an accuracy in the range 180–700 μm.

Appendix. Radiation source scheme in the proposed tomograph

The probe radiation source (*1*) (Fig. 1) intended for use in the tomograph considered in this study should meet a number of requirements. It should ensure, first, the formation of tomograms of a medium in different spectral ranges in a sufficiently

broad wavelength range and, second, the highest possible resolving power in terms of the Rayleigh criterion in each zone. To this end, it is necessary that the wavelengths of THz waves emitted in the kth zone of this range lie in the interval

$$(\lambda_k - \Delta\lambda_k/16) - (\lambda_k + \Delta\lambda_k/16), \quad \text{(A1)}$$

where λ_k is the centre wavelength of the interval and $\Delta\lambda_k = \lambda_k/8$ is its width. Third, the THz generator should excite THz waves within a region of diameter $d_g \ll \lambda_k$. If the last condition is met, the region is essentially a point source of THz waves, emitting a broadband spherical wave. From this wave, several narrow-band spherical waves should be separated out, with centre wavelengths λ_k and bandwidths $\Delta\lambda_k = \lambda_k/8 \ll \lambda_k$. The coherence length ($L_{ck}$) and the resolving power in terms of the Rayleigh criterion (R_k) in the kth interval are then given by

$$L_{ck} = \lambda_k^2/\Delta\lambda_k = 8\lambda_k,\ R_k = L_{ck}/4 = 2\lambda_k. \quad \text{(A2)}$$

The above requirements for the source (*1*) can be satisfied by using a broadband THz generator based on a femtosecond laser. Such a generator emits sufficiently intense THz waves in the range 90–350 μm [8]. A prism spectroscope decomposes the entire emission spectrum in this range into separate portions [13]. Using the relation for the wave dispersion in the dielectric material of the spectroscope's prism,

$$n'(\lambda_k) = \lambda_k/(\Delta\lambda_k t_p), \quad \text{(A3)}$$

where $t_p = 8$ mm is the prism base size [13], and taking into account that $\Delta\lambda_k = \lambda_k/8$, we obtain

$$n'(\lambda_k) = n'(\lambda_1) = 10\ \text{cm}^{-1}. \quad \text{(A4)}$$

Using (A3) and (A4), we find that refracted waves emerge from the prism at angles $\beta_k = n'(\lambda_k)\lambda_k = 10\ \text{cm}^{-1}\times\lambda_k$ to the direction of the beam incident on the prism [13]. As the first spectral interval, we take the interval with the shortest centre wavelength λ_1, 100 μm, and the corresponding bandwidth

$$\Delta\lambda_1 = \lambda_1/8 \approx 12\ \mu\text{m}. \quad \text{(A5)}$$

It follows from Eqns (A1)–(A5) that, in this interval, the source (*1*) (Fig. 1) will emit a narrow-band spherical wave at an angle $\beta_1 = 10^{-1}$ rad, with a centre wavelength $\lambda_1 = 100$ μm, bandwidth $\Delta\lambda_1 = \lambda_1/8 \ll \lambda_1$ and coherence length $L_{c1} = \lambda_1^2/\Delta\lambda_1 = 800$ μm.

A schematic of the source (*1*) is presented in Fig. 1A. A THz generator (*1*) excites a broadband spherical THz wave (*3*) in a region (*2*) of diameter $d_g \approx 20$ μm ($d_g \ll \lambda_1$). The wave travels through the input aperture (*4*) of a prism spectroscope (*5*) to a lens (*6*) with a focal length $f_1 = 18$ mm. The lens (*6*) transforms the spherical wave (*3*) into a plane wave, which propagates to the prism (*7*), with a base size $t_p = 8$ mm and height $h_p = 6$ mm. The narrow-band plane waves emerging from the prism (*7*) (angles of refraction $\beta_k = 10\ \text{cm}^{-1}\times\lambda_k$) have centre wavelengths λ_k and bandwidths $\Delta\lambda_k = \lambda_k/8$. The waves then propagate to a lens (*8*) with a focal length $f_2 = 60$ mm and the same diameter as that of lens *6*. Lens *8* focuses the waves onto its focal plane, forming several real images of region *2*. Lenses *6* and *8* are located symmetrically about the dashed line AB.

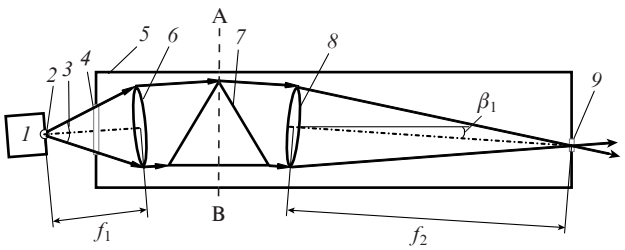

Figure 1A. Schematic of the radiation source in the proposed tomograph: (*1*) THz generator; (*2*) region in which a broadband spherical THz wave (*3*) is excited; (*4*) input aperture of a prism spectroscope (*5*); (*6*) lens with a focal length $f_1 = 18$ mm; (*7*) prism; (*8*) lens with a focal length $f_2 = 60$ mm; (*9*) output aperture of the probe radiation source.

In the initial position, the prism (*7*) should be positioned so that its central axis (dashed line in Fig. 1A) is parallel to the input aperture (*4*). As shown earlier [13], the image at the centre wavelength λ_1 is then located at the intersection of the optical axis of lens *8* (dot-dashed line in Fig. 1A) with the front focal plane of this lens at an angle $\beta_1 = \lambda_1/d_s$, where d_s is the diameter of lenses *6* and *8*. It can be shown that this image has the form of an Airy disc with a central zone diameter $d_1 \approx 1.2$ mm. A circular diaphragm (*9*) of the same diameter d_1 placed in this zone serves as an output aperture of the probe radiation source when the prism (*7*) is in its initial position. It can also be shown that the diaphragm (*9*) transmits only wavelengths in the band $\Delta\lambda_1 = \lambda_1/8 \approx 12$ μm.

It follows from Eqns (A1)–(A5) that the first spectral interval ($k = 1$) ensures the following four parameters of the THz source: $\lambda_1 = 100$ μm, $\Delta\lambda_1 = 94$–106 μm, $L_{c1} = 800$ μm and $d_1 = 1.2$ mm. The initial tomogram formed at the wavelength λ_1 has the best possible resolving power of the tomograph in this interval: $R_1 = L_{c1}/4 = 200$ μm.

In the other spectral intervals in the wavelength range 90–350 μm, tomograms are formed in a similar way. The corresponding parameters are listed in Table 1A.

Table 1A. Parameters of the tomograph.

Centre wavelength λ_k/μm	Bandwidth $\Delta\lambda_k$/μm	Coherence length L_{ck}/μm	Resolving power R_k/μm	Prism angle β_k/rad.
100	94–106	800	200	0
113	106–120	904	226	0.013
128	120–136	1024	256	0.015
148	139–157	1184	296	0.2
174	163–185	1392	348	0.26
209	196–221	1672	418	0.035
262	196–278	2096	524	0.053
329	308–350	2632	658	0.067

References

1. Bouma B.E., Tearney G.J. (Eds) *Handbook of Optical Coherency Tohography* (New York: Marsel Dekker, 2002).
2. Tuchin V.V. (Ed.) *Handbook of Optical Biomedical Diagnostics* (Bellingham: SPIE press, 2002).
3. Kirillin M.Yu., Meglinski I.V., Priezzhev A.V. *Kvantovaya Elektron*., **36**, 247 (2006) [*Quantum Electron*., **36**, 247 (2006)].
4. Veksler B.A., Kuz'min V.L., Kobzev E.D., Meglinski I.V. *Kvantovaya Elektron*., **42**, 394 (2012) [*Quantum Electron*., **42**, 394 (2012)].
5. Mandrosov V.I. *Nelineinyi Mir*, **8** (6), 361 (2010).
6. Klimenko I.S. *Golografiya sfokusirovannykh izobrazhenii i spekl-interferometriya* (Focused-Image Holography and Speckle Interferometry) (Moscow: Radio i Svyaz', 1985).
7. Cherkasova O.P., Kuritzin I.I., Mandrosov V.I., Nazarov M.M., Shkurinov A.P. *Abst. 2-nd Int. Conf. 'Terahertz and Microwave Radiation: Generation, Detection and Applications' (TERA 2012)* (Moscow, 2012) p. 102.
8. Kuleshov E.R., Nazarov M.M., Shkurinov A.P., Tuchin V.V. *Kvantovaya Elektron*., **38**, 647 (2008) [*Quantum Electron*., **38**, 647 (2008)].
9. Bakut P.A., Mandrosov V.I. *Kvantovaya Elektron*., **37**, 81 (2007) [*Quantum Electron*., **37**, 81 (2007)].
10. Kuritsyn I.I., Mandrosov V.I., Shkurinov A.P., Nazarov M.M., Cherkasova O.P. *Kvantovaya Elektron*., **43**, 958 (2013) [*Quantum Electron*., **43**, 958 (2013)].
11. Denisyuk Yu.N. *Opt. Spektrosk*., **15**, 522 (1963).
12. Mandrosov V. *Coherent Fields and Images in Remote Sensing* (Bellingham: SPIE press, 2004) Vol. PM130.
13. Born M., Wolf E. *Principles of Optics* (Oxford: Pergamon, 1969; Moscow: Nauka, 1973).